Atomic mobility in calcium and sodium aluminosilicate melts at 1200 °C

Corinne Claireaux Claireaux, Marie-Hélène Chopinet, Ekaterina Burov, Emmanuelle Gouillart, Mathieu Roskosz, Michael J. Toplis

Atomic mobility in calcium and sodium aluminosilicate melts at 1200°C

Corinne Claireaux[a], Marie-Hélène Chopinet[a], Ekaterina Burov[a], Emmanuelle Gouillart[a], Mathieu Roskosz[b], Michael J. Toplis[c]

[a] *Surface du Verre et Interfaces (UMR 125), CNRS/Saint-Gobain Recherche, 39 quai Lucien Lefranc, 93300 Aubervilliers, France*
[b] *Muséum National d'Histoire Naturelle, Institut de Minéralogie, de physique de la matière condensée et de cosmochimie, Sorbonne University, Paris, France*
[c] *Laboratoire Dynamique Terrestre et Planétaire (UMR 5562), Observatoire Midi-Pyrénées, 14 avenue Belin, Toulouse, 31400, France*

Abstract

Multicomponent chemical diffusion in liquids of the quaternary system $CaO–Na_2O–Al_2O_3–SiO_2$ has been studied. Diffusion-couple experiments were performed at 1200°C and for different durations around a central composition of 64.5 wt%SiO_2 , 13.3 wt%Na_2O, 10.8 wt%CaO, 11.4 wt%Al_2O_3, leading to an overconstrained system of equations that was used to determine the diffusion matrix of the system. The dominant eigenvector of the diffusion matrix was found to correspond to the exchange between sodium and calcium, consistent with the results of the ternary soda-lime silica system. On the other hand, neither of the other two eigenvectors of the diffusion matrix of the quaternary system involve sodium. Given a factor of 50 between the dominant and second eigenvalue, diffusion couples involving the exchange of sodium oxide and a network-forming oxide result in strong uphill diffusion of calcium. The second eigenvector, corresponding to the exchange of calcium with silicon and aluminum, is close to the dominant eigenvector found in previous studies of ternary alkaline-earth aluminosilicate systems. Our results therefore suggest that simple systems may be used to understand diffusive mechanisms in more complex systems.

1. Introduction

Chemical diffusion in silicate and aluminosilicate melts plays a key role in mass transfer processes of importance in the Earth and planetary sciences, as well as in applied fields such as industrial glass making (Schaeffer, 1984). Diffusive mechanisms involved in crystal-melt interactions have been studied both for mineral dissolution (Edwards and Russell, 1996; Liang, 1999; Acosta-Vigil et al., 2002, 2006; Chen and Zhang, 2008), refractory corrosion (Samaddar et al., 1964; Oishi et al., 1965; Sandhage and Yurek, 1990) or crystal nucleation and growth (Roskosz et al., 2005, 2006). In addition, the link between diffusive and viscous transport has received considerable attention (Mungall, 2002; Njiokep et al., 2008; Ni et al., 2015), and diffusion has also been shown to influence isotope fractionation (Richter et al., 1999, 2008), onset of boundary layer convection (Spera et al., 1984; Liang et al., 1994), melt oxidation (Cooper et al., 1996; Smith and Cooper, 2000; Behrens and Stelling, 2011) and phase separation (Mazurin and Porai-Koshits, 1984).

The multicomponent nature of chemical diffusion is a key element of diffusion in silicate melts, as underlined by phenomena such as uphill diffusion (Liang et al., 1996a) or the mixed-alkali effect (Imre et al., 2002). In a polymerized silicate or aluminosilicate network, the common picture of random jumps of individual particles converts to consideration of cooperative rearrangements that involve several species (Mungall, 2002). Although effective binary diffusion coefficients may provide a convenient representation of some diffusive mechanisms, a more thorough description is provided by the *diffusion matrix* (Zhang, 2010; Liang, 2010), that links the flux of a given element to all the independent concentration gradients. The eigenvectors of the diffusion matrix provide a macroscopic indication of the exchange chemistry that dominates at the microscopic level, while the associated eigenvalues provide an indication of the relative frequencies of those exchanges (Zhang, 2010; de Koker and Stixrude, 2010).

Due to the large amount of experimental data required, studies that determine the complete diffusion matrices in silicate melts represent a small

Email address: emmanuelle.gouillart@saint-gobain.com (Emmanuelle Gouillart)

fraction of the large body of literature that exists concerning diffusion in molten silicates. Of those studies, work has concentrated on $CaO-Al_2O_3-SiO_2$, a simplified system of wide geological interest (Liang and Davis, 2002; Liang et al., 1996b; Oishi et al., 1982; Sugawara et al., 1977). Other studies in ternary systems have been performed in the systems $MgO-Al_2O_3-SiO_2$ (Kress and Ghiorso, 1993; Richter et al., 1998), $K_2O-Al_2O_3-SiO_2$ (Chakraborty et al., 1995a,b) and $SrO-SiO_2-K_2O$ (Varshneya and Cooper, 1972) and in $Na_2O-CaO-SiO_2$ (Wakabayashi and Oishi, 1978; Trial and Spera, 1994), a soda-lime composition of interest to glass-makers. Very few studies have addressed more complex systems, exceptions being $CaO-MgO-Al_2O_3-SiO_2$(Kress and Ghiorso, 1993; Richter et al., 1998) and $K_2O-Na_2O-Al_2O_3-SiO_2-H_2O$ (Mungall et al., 1998). Surprisingly, no aluminosilicate composition containing both alkali and alkaline earth has been explored to determine its diffusion matrix, despite the fact that geological melts contain aluminum as well as alkali and alkaline-earth elements, and despite the industrial interest of the $CaO-Na_2O-Al_2O_3-SiO_2$ system. Furthermore, the link between preferential exchanges expressed by eigenvectors in simplified (such as ternary) systems, and exchanges in more complex systems, remains to be studied.

The objective of this work is to determine the diffusion matrix of the quaternary $CaO-Na_2O-Al_2O_3-SiO_2$ system, in the peralkaline domain. From the diffusion matrix, we aim at deriving its eigenvectors in order to understand diffusive transport in this quaternary system, and to compare its eigenspaces with other silicate and aluminosilicate systems.

2. Theoretical background on chemical diffusion

A description of the formalism of multicomponent chemical diffusion can be found in several references (Gupta and Cooper, 1971; Trial and Spera, 1994; Brady, 1995; Zhang et al., 2010; Liang, 2010). We reproduce the main arguments here, for the sake of completeness.

Self-diffusion -. Chemical diffusion of a single species, often considered to be a dilute tracer inside a matrix, is described by Fick's first law

$$\mathbf{j} = -D\nabla C, \tag{1}$$

that proposes a linear relation between the flux $\mathbf{j}$ and the concentration gradient ∇C. The linear coefficient D is called the diffusion coefficient or diffusivity of the element. Fick's first law can be derived from microscopic principles, by computing the flux of individual particles (atoms, ions, molecules...) subject to thermally-activated random motion. Assuming that diffusion is the only source of local concentration changes, i.e. in the absence of convection (Richter et al., 1998) or chemical reaction (Cooper et al., 1996; Smith and Cooper, 2000), and that the diffusion coefficient does not vary with the concentration of the species, one obtains Fick's second law:

$$\frac{\partial C}{\partial t} = D\nabla^2 C, \tag{2}$$

also known as the diffusion equation. In silicate melts, diffusion of single species has been measured (Jambon and Carron, 1976; Jambon, 1982; Liang et al., 1996a; LaTourrette et al., 1996; Zhang et al., 2010; Lesher, 2010; Wu et al., 2012) and modeled (Mungall, 2002; Zhang, 2010) for a large variety of compositions and elements.

Diffusion matrix-. The motion of species in silicate melts depends on their environment, so that a complete description of diffusion has to take into account couplings between species. For a mixture of n species, such couplings may be described by a *diffusion matrix*, that extends Fick's first law to its vectorial formulation:

$$\mathbf{j} = -\mathbf{D}\nabla\mathbf{C}, \tag{3}$$

where $\mathbf{C} = (C_1, \ldots, C_n)$ is the vector of local concentrations, $\mathbf{j} = (\mathbf{j}_1, \ldots, \mathbf{j}_n)$ represents the fluxes, and $\mathbf{D}$ is the $n \times n$ diffusion matrix. With this formalism, the flux of one species depends on the gradient of all components:

$$\mathbf{j}_i(\mathbf{x}) = -\sum_k D_{ik}\nabla C_k(\mathbf{x}). \tag{4}$$

A more complex formulation could include even more components than the n chemical concentrations, for example by distinguishing between the possible speciations of network formers, that influence the local displacement of ions. Nevertheless, since chemical concentrations are more easily accessed with a good spatial resolution than other quantities, only chemical concentrations are usually considered as components.

Furthermore, it is possible to reduce the dimensionality of the diffusion matrix for systems satisfying the conservation of mass. If the C_i are mass concentrations,

and if we neglect variations of density with composition (an approximation that will be made here), then

$$\sum_i C_i(\mathbf{x}) = 100. \tag{5}$$

Taking the spatial derivative of the above equation results in

$$\sum_i \nabla C_i(\mathbf{x}) = 0. \tag{6}$$

Because of the above constraint, the gradient vector $\nabla\mathbf{C}$ belongs to a hyperspace of dimension $n-1$. Since $\mathbf{D}$ can only be measured through its effect on $\nabla\mathbf{C}$, it is only possible to measure $(n-1)\times(n-1)$ independent coefficients of $\mathbf{D}$. Therefore, $\mathbf{D}$ is often defined as an $(n-1)\times(n-1)$ matrix. The n^{th} species is considered to be dependent on the others; it is usually chosen among network formers, that are less mobile, although formally any species can be chosen as the dependent one.

Finally, a vector formulation of Fick's second law is obtained, under the assumption that $\mathbf{D}$ is independent of concentrations

$$\frac{\partial\mathbf{C}}{\partial t} = \mathbf{D}\nabla^2\mathbf{C}. \tag{7}$$

Measuring the diffusion matrix -. The diffusion matrix is typically computed from 1-D diffusion experiments between two melts of different initial compositions, with a flat interface. At $t = 0$, the concentration gradient is therefore nonzero only at the interface between the two liquids:

$$\nabla\mathbf{C} = \mathbf{\Delta C}\delta(x), \tag{8}$$

where $\mathbf{\Delta C}$ is the step of concentration between the two slabs, the interface is taken at $x = 0$, and

$$\delta(x) = \begin{cases} 1 & \text{if } x = 0 \\ 0 & \text{if } x \neq 0. \end{cases} \tag{9}$$

Eq. (7) with the initial condition of Eq. (8) can be solved analytically in the eigenbasis of the diffusion matrix. Let us define

$$\mathbf{D} = \mathbf{P}\mathbf{\Lambda}\mathbf{P}^{-1}, \tag{10}$$

with

$$\mathbf{\Lambda} = \begin{pmatrix} \lambda_1 & \dots & \dots \\ \vdots & \ddots & \dots \\ \vdots & \vdots & \lambda_{n-1} \end{pmatrix} \tag{11}$$

the diagonal matrix of eigenvalues λ_i, and $\mathbf{P} = (\mathbf{v}_1, \dots, \mathbf{v}_{n-1})$ is the block matrix of the eigenvectors $\mathbf{v}_i$. Therefore,

$$\mathbf{\Lambda}\mathbf{v}_i = \lambda_i\mathbf{v}_i. \tag{12}$$

Defining $\tilde{\mathbf{C}} = \mathbf{P}^{-1}\mathbf{C}$ and $\mathbf{\Delta}\tilde{\mathbf{C}} = \mathbf{P}^{-1}\mathbf{\Delta C}$, respectively the concentration and the initial concentration step in the eigenbasis of $\mathbf{D}$, Eq. (7) can be written as

$$\frac{\partial\tilde{\mathbf{C}}}{\partial t} = \mathbf{\Lambda}\nabla^2\tilde{\mathbf{C}}. \tag{13}$$

Since $\mathbf{\Lambda}$ is a diagonal matrix, all equations of (13) are independent and have similar solutions to that obtained for the diffusion of a single species:

$$\tilde{C}_i(x,t) = \Delta\tilde{C}_i \,\mathrm{erf}\left(\frac{x}{\sqrt{2\lambda_i t}}\right). \tag{14}$$

Note that the above solution is valid for an infinite medium, *i.e.* when the width of the diffusing interface is much smaller than the width of each sample. From an experimental set of concentration profiles, the diffusion matrix is obtained by fitting theoretical profiles of Eq. (14) to the experimental profiles.

3. Materials and methods

3.1. Experimental methods

Glass compositions -. We choose to measure the diffusion matrix in a composition domain centered on the peralkaline composition $\mathbf{C}_0$ = 64.5 wt%SiO_2, 13.3 wt%Na_2O, 10.8 wt%CaO, 11.4 wt%Al_2O_3 (corresponding to $\mathbf{C}_0$ = 67.4 mol%SiO_2, 13.5 mol%Na_2O, 12.1 mol%CaO, 7.0 mol%Al_2O_3, or $Si_{2.02}Na_{1.62}Ca_{0.73}Al_{0.28}O_6$). With this central composition, all compositions of diffusion-couple glasses lie in the peralkaline domain, while the concentration of all four oxides is important enough to allow for accurate measurements of the composition using electron microprobe analysis. Compared to window-glass soda-lime compositions, this composition is aluminum-enriched, a fact that generally increases the strength of the glass (Eagan and Swearekgen, 1978). Indeed, the composition studied here is close to industrially-used high-strength glass compositions (Karlsson et al., 2010; Danielson et al., 2016), such as compositions used in the aeronautic industry (Chopinet et al., 2001).

We prepared a set of glasses centered on $\mathbf{C}_0$ for the diffusion couple experiments. Choosing the concentration difference in a diffusion couple is a trade-off between two contradicting aspects: we expect the diffusion matrix to be independent of concentration only in

a small domain, while increasing the signal over noise ratio of concentration profiles requires to have a larger initial step of concentration. Here we choose a maximal concentration difference of 5wt%. We prepared 12 different glasses, each of them being enriched in one oxide and depleted in another one with respect to $\mathbf{C}_0$. For example, we denote as AN a composition with 2.5wt% more alumina, and 2.5wt% less sodium oxide than $\mathbf{C}_0$.

Glasses were synthesized from raw materials of industrial grade, using Ronceveaux sand and Tacon limestone from Samin, hydrated alumina from Dadco, and sodium carbonate from Novacarb. 0.3wt% of sodium sulfate and 300 ppm of coke were added as fining agents. In addition, 100 ppm of cobalt oxide were added to one glass in each diffusion couple, in order to detect convection. Raw materials were weighed and mixed for several minutes in a Turbula-type mixer, and melted for 6h in a 800 mL platinum crucible in a Joule-heated furnace at 1500°C. Melts were mixed for one hour with a platinum stirrer to improve homogeneity. Melts were then quenched on a metallic plate, and annealed at 600° C for one hour. Compositions of the different glasses are given in Table 1. We have also reported in Table 1 densities of the different compositions estimated at 1200°C using the models of (Bottinga et al., 1982), (Spera, 2000), (Priven, 2004) and (Fluegel et al., 2008). Values given in Table 1 correspond to the average of density values for the different models. The standard deviation of the density between models is smaller than 0.02 for all models, and the standard deviations of the difference of density between endmembers is smaller than 0.007 for all experiments but one (AC/CA, with a standard deviation of 0.017). Relative variations of calculated density between diffusion endmembers are all smaller than 2.5%, confirming the validity of mass conservation along a diffusion profile.

Diffusion experiments -. We performed diffusion experiments for each couple intersecting at $\mathbf{C}_0$, resulting in 6 different diffusion couples: NA/NA, CA/AC, AS/SA, CN/NC, CS/SC, and NS/SN (using the notation defined above, with the first letter denoting the element in excess and the second letter the element that is depleted). Therefore, only two oxides have a significant concentration difference between the two endmembers of a given diffusion couple.

In theory, only $(n-1)$ experiments with $(n-1)$ profiles each are required to determine the $(n-1)^2$ coefficients of the diffusion matrix. However, more experiments than this bare minimum are useful to overconstrain the solution in the case of noisy data. Furthermore, our set of experiments is completely symmetrical with respect to the different oxides, so that we explore all the possible directions of exchange between oxides.

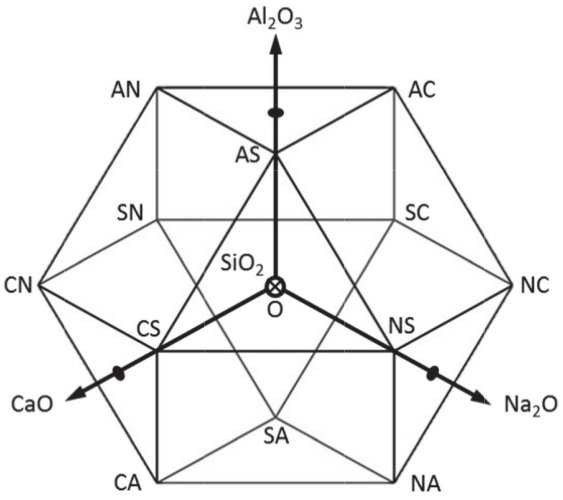

Figure 1: Schematic of diffusion-couple compositions.

Diffusion experiments were made at 1200°C, a temperature low enough to avoid convection and high enough to avoid crystallization. Square slabs of dimensions $15\times15\times5$ mm^3 of the different glasses were cut; a coarse polishing of surfaces ensured a good contact between the two slabs, limiting the formation of bubbles. Slabs were put in vitreous silica crucibles of 25-mm diameter, the denser glass being placed below the lighter one. The space between the crucible and the glass slabs was filled with quartz sand to limit slumping of the melt, and to mitigate the formation of cracks during quenching. Crucibles were introduced into an electric furnace preheated at 1200°C. Samples reached 1200°C about 20 minutes after being put inside the furnace. Therefore, we define $t = 0$ as the end of this 20-minute period. Counting from this point, isothermal treatments of durations of 20 minutes, 1 hour and 3 hours were performed for all diffusion couples. Samples were then quenched in air and annealed at 600° C for one hour to avoid fracture during subsequent sample preparation. They were then mounted in epoxy resin, cut perpendicularly to the interface, and polished to optical quality for further observation.

Diffusion profiles -. The absence of convection was verified using optical microscopy (using color contrast thanks to cobalt oxide) as well as scanning electron microscopy in back-scattered mode, on a Zeiss Gemini DSM 982 FEG-SEM. Although convection was absent in most experiments, two of the 3-hour experiments had to be discarded because of interfaces disturbed by con-

	$\mathbf{C}_0$	AC	AN	AS	CA	CN	CS	NA	NC	NS	SA	SC	SN
Na_2O	13.3	13.7	**10.8**	13.5	13.6	**10.5**	13.3	**16.0**	**15.9**	**15.4**	13.6	13.2	10.4
CaO	10.8	**7.8**	10.7	10.2	**13.7**	**13.8**	**13.6**	10.7	**7.9**	11.7	10.6	**6.9**	10.6
Al_2O_3	11.4	**13.4**	**13.3**	**13.5**	**8.4**	12.0	11.4	**8.9**	11.6	10.8	**8.9**	11.7	11.7
SiO_2	64.5	65.1	65.4	**62.1**	64.3	63.6	**61.7**	64.3	64.6	**62.0**	**66.9**	**66.7**	**66.8**
density		2.35	2.38	2.37	2.36	2.40	2.40	2.37	2.35	2.38	2.36	2.34	2.37

Table 1: Compositions (in weight percents) and calculated densities ($\times 10^3$ kg.m^{-3}) of glasses used in diffusion couples. Chemical compositions were measured for each glass from the average of 20 electron microprobe analysis measurements. $\mathbf{C}_0$ is a theoretical composition (no glass of composition $\mathbf{C}_0$ was synthetized).

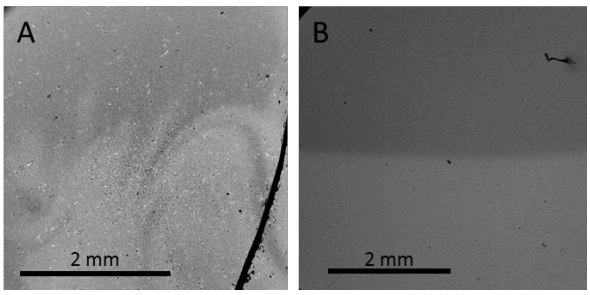

Figure 2: SEM images of interfaces between diffusion endmembers. (a) Interface destabilized by convection, that is discarded. (b) Stable interface for which diffusion only has been at play.

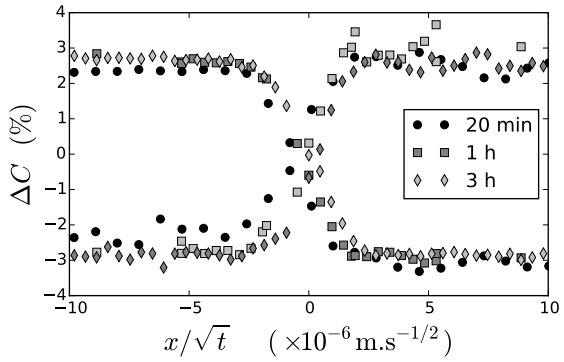

Figure 3: CS-SC exchange - Calcium oxide and silica concentration versus normalized distance to the interface $x/\sqrt{t}$, for diffusion experiments of 20 minutes, 1 hour and three hours.

vection (see Fig. 2). Diffusion profiles were measured using a Cameca SX-100 electron microprobe at the University of Lille. Analyses were performed for 20 seconds with an acceleration voltage of 15 kV, a current of 15 nA and a spot size of 20 microns in order to reduce the charge density on the sample. For an accurate measurement of sodium concentration, four counting intervals of 5 seconds were used, and a regression performed to extrapolate decreasing concentrations back to the initial concentration. Measurement accuracy on sodium oxide is of the order of 1 wt%, while that of the other elements is of the order of 0.2 wt%. Along a diffusion profile, two measurement points were always separated by at least 30 microns to limit the impact of sodium migration at one point on adjacent measurements.

3.2. Mathematical analysis of diffusion profiles

We first verified that diffusion profiles obtained for different durations on the same diffusion couple could be overlain when plotting concentrations versus rescaled distance $x/\sqrt{t}$. A typical example is plotted in Fig. 3, for the SC/CS diffusion couple, where a good agreement is observed between the different times. Rescaled profiles corresponding to the shortest time (20 minutes) are slightly shifted compared to rescaled profiles for one and three hours. This small difference likely originates from the uncertainty concerning the starting time. Therefore, in the following we only use the 1- and 3-hour experiments to obtain the diffusion matrix, corresponding to a set of 10 experiments.

In order to obtain the diffusion matrix, we perform a least-square minimization of the difference between experimental concentration profiles, and concentrations resulting from Eq. (14). Least-square minimization is the standard method to fit diffusion matrices (Trial and Spera, 1994; Liang et al., 1996a; Acosta-Vigil et al., 2002; Liang, 2010), since it allows one to fit, at the same time, a large number of profiles. It is also more robust to noise than direct methods such as the Boltzmann-Matano method (Kress and Ghiorso, 1995; Lesher, 1994; Saggioro and Ziemath, 2006; Liang, 2010; Vielzeuf and Saúl, 2011), that requires the calculation of spatial derivatives of the profiles.

We use the optimization routine `optimize.leastsq` provided by the Python package `scipy`, that implements the Levenberg-Marquardt algorithm. The difference to be minimized is computed in the eigenbasis of the diffusion matrix. Therefore, at each iteration of the minimization procedure, a new set of eigenvectors and eigenvalues of $\mathbf{D}$ is obtained, allowing one to trans-

form experimental concentration profiles to profiles in the new eigenbasis, that are compared to theoretical profiles defined by Eq. (14). Silica is used as the dependent species. Since the fitting procedure involves 9 parameters, and the non-linear function to be minimized is not convex and can have several local minima, special care is required for the initialization of **D**. Initial parameters for **D** are selected visually from a rough adjustment of experimental and computed concentration profiles.

4. Results

4.1. Diffusion profiles

Fig. 4 represents diffusion profiles for all diffusion couples, for a thermal treatment of one hour. Several observations can be made from this set of profiles. Diffusion distances from a few hundreds of microns to one millimeter are observed, confirming that the electron microprobe is a technique perfectly adapted to our experiments. Also, the maximum diffusion distance is of the order of one millimeter, much smaller than the height of the original glass sample (5 mm), so that the approximation of diffusion in an infinite medium is valid here. Experiments with an initial difference of sodium oxide show a larger diffusion width than experiments with the same concentration of sodium oxide for the two melts. Sodium being the most mobile species, this result is to be expected. Uphill diffusion of calcium is observed in the case of exchange between sodium and a network formers, that is for the NA/AN and NS/SN couples. Uphill diffusion of calcium is also observed for the AS/SA couple, for which there exists as well a small concentration difference in sodium oxide between end members. In such experiments, diffusion profiles of different elements have very different diffusion widths, the diffusion distance of sodium and calcium being much greater than that of silicon and aluminum.

4.2. Diffusion matrix

Using the optimization procedure described in the previous section, we obtained the diffusion matrix from concentration profiles available for 1- and 3-hour experiments at 1200° C. With SiO_2 as the dependent component, the matrix **D** is given by

$$\mathbf{D} = \begin{pmatrix} 25.55 & -4.45 & -8.29 \\ -22.86 & 4.85 & 8.00 \\ 0.33 & -0.29 & -0.02 \end{pmatrix},$$

where the lines of **D** give the fluxes of Na_2O, CaO, and Al_2O_3 respectively, and coefficients are in $10^{-12}m^2.s^{-1}$ units. Since coefficients of the fitted 3×3 matrix **D** represent differences between the "true" coefficients of the unknown 4×4 matrix, we also give here the eigenvalues and eigenvectors of **D**, that are the same regardless of the choice of the dependent species. Eigenvalues and eigenvectors are shown in Table 2. Since the coefficients of eigenvectors can be multiplied by any constant value, we set the principal coefficient to 1, for the sake of clarity. Uncertainties on the different coefficients were obtained using a procedure known as *bootstrapping* in statistics, relying on random sampling with replacement: one profile is excluded in turns from the set of profiles, in order to compute different estimations of the diffusion matrix. We selected the excluded profiles in the set of experiments for which we had both data for 1 and 3 hours, in order to keep data corresponding to all diffusion couples within the fitting set. Excluding a diffusion couple resulted in a larger deviation for eigenvalues and eigenvectors; this observation validates our experimental strategy to use all 6 diffusion couples, although in theory 3 would have been enough to constrain the fitting procedure. While previous studies (Chakraborty et al., 1995a,b) have suggested that a minimum number of profiles is sufficient to determine the diffusion matrix, we believe that a smaller set of experiments comes at the cost of large uncertainties on the diffusion matrix (Liang, 2010).

Table 2: Eigenvalues ($\times 10^{-12} m^2.s^{-1}$) and eigenvectors

	$\mathbf{v}_1$	$\mathbf{v}_2$	$\mathbf{v}_3$
α_i	29.5 ± .2	0.58 ± 0.02	0.3 ± .06
Na_2O	1	0.02 ± 0.01	−0.15 ± 0.01
CaO	−0.92 ± 0.005	1	0.98 ± 0.04
Al_2O_3	0.02 ± 0.01	−0.47 ± 0.06	−1 ± 0.03
SiO_2	−0.09 ± 0.02	−0.52 ± 0.08	0.17 ± 0.05

4.3. Eigenvectors and eigenvalues

The dominant eigenvector of the diffusion matrix, associated to the fastest diffusion process, is found to correspond to the exchange of sodium and calcium. The second eigenvector corresponds to the exchange of calcium with silicon and aluminum, while the third eigenvector is dominated by the exchange of calcium and aluminum. Therefore, the two diffusion processes highlighted by the minor eigenvectors involve no or very little sodium, and they are much slower. The ratio between the first and the second eigenvalue is on the order of 50. For silicates, such high ratios between eigenvalues have only been reported in systems with alkalis: Trial and Spera (Trial and Spera, 1994) found a ratio of 24 in the NCS system, and also had a first eigenvector

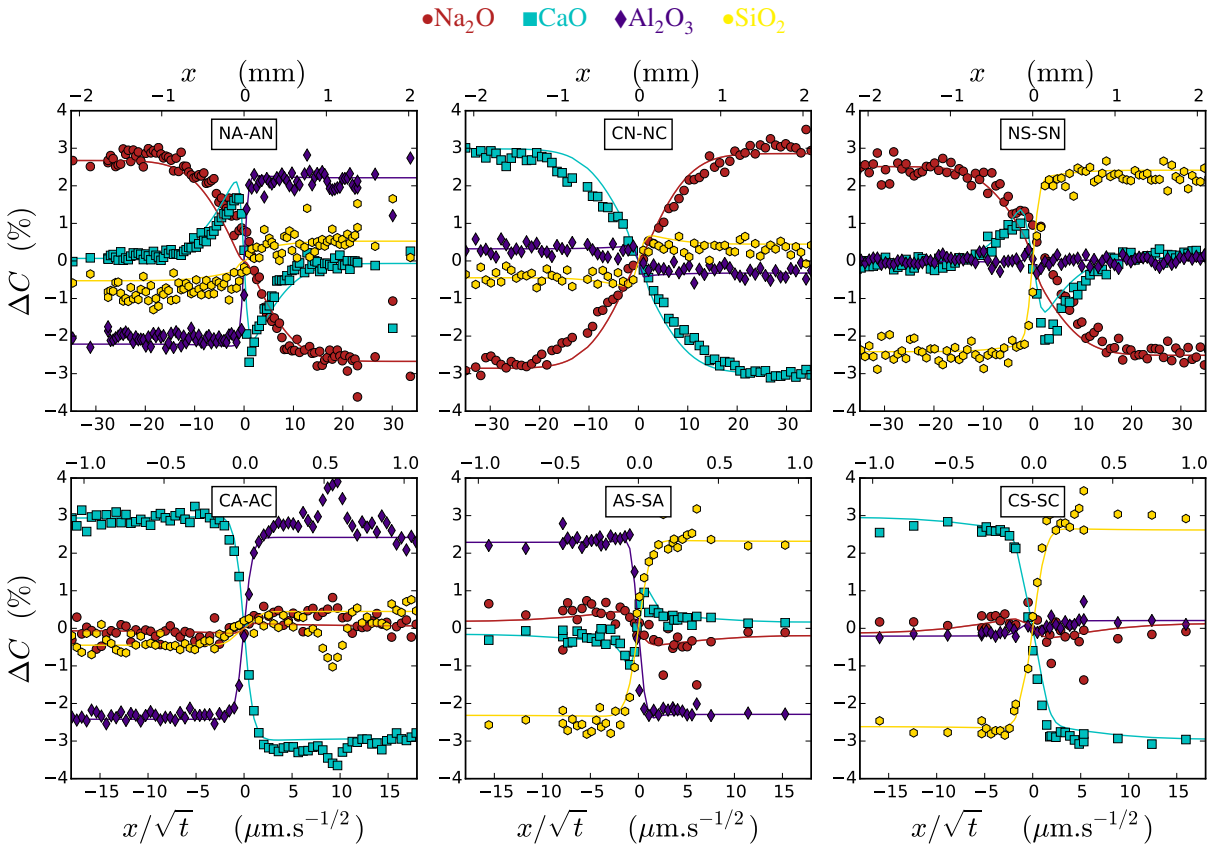

Figure 4: Concentration profiles for all diffusion couples at 1200°C and 1-hour treatments. Note the different spatial scale for diffusion couples involving sodium (first line) and not involving sodium (second line). Spatial coordinates are given both in mm and in rescaled units.

colinear to sodium-calcium exchange. Chakraborty et al. (Chakraborty et al., 1995a,b) found ratios between 5 and 270 for the KAS system. Nevertheless, the latter experiments used only one diffusion couple to fit a diffusion matrix, making it hard to quantify the terms of the diffusion matrix accurately, all the more for an ill-conditioned matrix (with very different eigenvalues). In contrast, systems involving only alkaline-earth network modifiers (Kress and Ghiorso, 1993; Liang et al., 1996b; Richter et al., 1998), including systems involving both Ca and Mg (Kress and Ghiorso, 1993; Richter et al., 1998), have been found to have eigenvalues of the same order of magnitude, with a ratio smaller than 5 between the largest and second largest eigenvalues.

The decoupling between α_1 and α_2 has important consequences for all diffusion paths, that is the set of compositions linking endmembers in the course of a diffusion experiment. In Fig. 5, we have represented the diffusion paths in the 3-D space of compositions (the 4th component being known from mass conservation). All diffusion paths cross at $\mathbf{C}_0$, the average composition. We have also represented the three eigenvectors of the diffusion matrix. As shown in Fig. 5, for any diffusion couple with a non-null projection on the dominant eigenvector (that is, any diffusion couple with $\Delta C_{\mathrm{Na}} \neq 0$), the diffusion path is mostly colinear to the dominant eigenvector (direction represented by the thick orange arrow). In other words, diffusion paths are aligned with the dominant eigenvector in regions where ΔC_{Na} is substantial, while they are aligned with the other eigenvectors (involving network formers) only when ΔC_{Na} is small.

5. Discussion

5.1. *Validity of the diffusion-matrix formalism*

While the overall quality of the fit of experimental data is satisfying, it can be noted in Fig. 4 that there is a slight asymmetry in the profiles of sodium and calcium, in the case of a difference of sodium concentration in

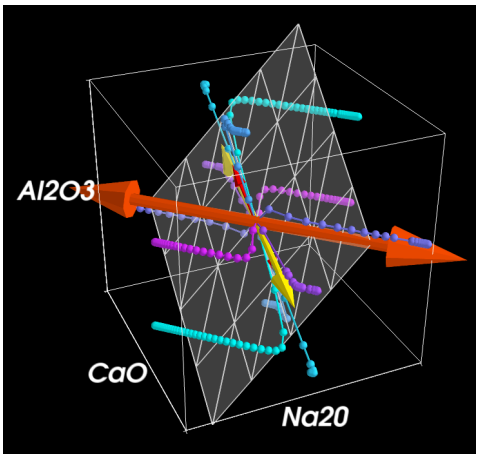

Figure 5: 3-D visualization of diffusion paths, centered around concentration $\mathbf{C}_0$. Concentrations can be represented in a 3-D Cartesian space, since the fourth concentration value can be deduced from the three other concentrations. The three axis represent a difference in Na_2O, CaO, and Al_2O_3, as shown by labels on the axes. The shaded white plane represents $\Delta C_{Na_2O} + \Delta C_{CaO} + \Delta C_{Al_2O_3} = 0$, so that deviations out of this plane represent a difference in silica concentration. Arrows (in orange, yellow and red) represent the directions of the eigenvectors of the diffusion matrix. Note that diffusion couples involving a difference in sodium oxide concentration are parallel to the dominant eigenvector at the two ends of the diffusion path.

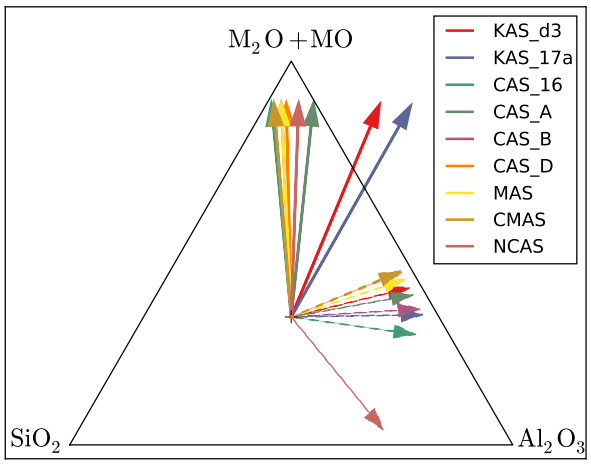

Figure 6: Directions of diffusion eigenvectors of Table 3, projected in the plane $\Delta C_{SiO_2} + \Delta C_{Al_2O_3} + \Delta C_{M_2O+MO} = 0$. Note that we have grouped together alkali M_2O and alkaline-earth MO oxides for more clarity, so that the dominant eigenvector of our NCAS system is not represented here. For all systems, the dominant eigenvector is represented with a solid line, while other(s) eigenvectors are represented with a dashed line. Note the persistence of an eigenvector corresponding to the exchange of alkali-earth oxides with an equal proportion of silica and alumina.

the diffusion couple. This asymmetry is probably due to variations of diffusion coefficient along the profile, possibly correlated to variations in melt viscosity generated by the composition gradient (i.e. Mungall (2002)). Accounting for the observed asymmetry would therefore require fitting diffusion profiles using a concentration-dependent diffusion matrix. Nevertheless, such refinement would only slightly modify the diffusion matrix quantified here, and was not attempted.

5.2. *Comparison with other systems*

In order to compare the eigenvectors of our quaternary system to other systems, the findings of several previous studies, in ternary or more complex systems are summarized in Tab. 3. For a graphical representation, we have plotted the directions of eigenvectors in Fig. 6.

Our dominant eigenvector, corresponding to the exchange of sodium and calcium, is similar to the principal eigenvector of the NCS system of Trial and Spera (Trial and Spera, 1994). Furthermore, this eigenvector has a much larger eigenvalue than the second eigenvector, in the two systems. In contrast, systems that have two alkalis (like the NKASH system of (Mungall et al., 1998)) or two alkaline-earth species (like the CMAS system of (Richter et al., 1998)) do not have an eigenvector corresponding to the fast exchange of these two alkali or two alkaline-earth species. This difference might be paralleled with slower transport properties (such as electrical conductivity) associated to the so-called mixed-alkali (Isard, 1969; Swenson and Adams, 2003) and mixed-alkaline-earth (Roling and Ingram, 2000; Kjeldsen et al., 2013) effects. These mixed effects have been assigned to a discrepancy between the sites of two alkali or two alkaline-earth species, with the consequence that the two species are "blocking" each other. It is also of note that the exchange between sodium and calcium was also found to be predominant in more complex geological melts (Lundstrom, 2003).

Moreover, sodium is present only in the dominant eigenvector, so that its diffusion is decoupled from network formers. This behaviour contrasts with systems with alkali species but no alkaline-earth species (Chakraborty et al., 1995b; Mungall et al., 1998), where alkalis exchange preferentially with silica rather than with alumina. However, an exchange of sodium with network formers might be followed by the faster exchange of calcium with sodium, along the direction of the dominant eigenvector, so that the exchange of sodium with network formers can be described by a combination of the two first eigenvectors.

As for our second eigenvector, corresponding to the exchange of calcium with similar quantities of silica and alumina, this exchange is close to the domi-

experiment	eigenvectors	eigenvalues ($\times 10^{-12} m^2.s^{-1}$)	T (° C)	reference
NCS	$Na_2O \leftrightarrow 0.85CaO + 0.15SiO_2$ $0.27Na_2O + 0.73CaO \leftrightarrow SiO_2$	105 4.4	1200	Trial and Spera (1994)
KAS D-3	$K_2O \leftrightarrow 0.14Al_2O_3 + 0.86SiO_2$ $0.75Al_2O_3 + 0.25K_2O \leftrightarrow SiO_2$	0.07 1×10^{-3}	1400	Chakraborty et al. (1995b)
KAS 17a	$K_2O \leftrightarrow 0.01Al_2O_3 + 0.99SiO_2$ $0.98Al_2O_3 + 0.02K_2O \leftrightarrow SiO_2$	10.8 0.04	1400	Chakraborty et al. (1995b)
KAS 23	$K_2O \leftrightarrow 0.02Al_2O_3 + 0.98SiO_2$ $0.8Al_2O_3 + 0.02K_2O \leftrightarrow SiO_2$	14.4 0.08	1600	Chakraborty et al. (1995b)
NKASH	$Na_2O \leftrightarrow SiO_2$ $K_2O \leftrightarrow SiO_2$ $Al_2O_3 + 0.08K_2O + 0.21Na_2O + 0.28H_2O \leftrightarrow 1.57SiO_2$ $H_2O \leftrightarrow SiO_2$	550 540 3.4 280	1600	Mungall et al. (1998)
CAS 16	$CaO \leftrightarrow 0.58Al_2O_3 + 0.42SiO_2$ $Al_2O_3 \leftrightarrow 0.15CaO + 0.85SiO_2$	99 23	1500	Liang et al. (1996a)
CAS A	$CaO \leftrightarrow 0.41Al_2O_3 + 0.59SiO_2$ $0.81Al_2O_3 + 0.19CaO \leftrightarrow SiO_2$	34 8.3	1500	Liang et al. (1996a)
CAS B	$CaO \leftrightarrow 0.54Al_2O_3 + 0.46SiO_2$ $0.93Al_2O_3 + 0.07CaO \leftrightarrow SiO_2$	47 23	1500	Liang et al. (1996a)
CAS D	$CaO \leftrightarrow 0.52Al_2O_3 + 0.48SiO_2$ $0.62Al_2O_3 + 0.38CaO \leftrightarrow SiO_2$	36 11	1500	Liang et al. (1996a)
MAS	$MgO \leftrightarrow 0.54Al_2O_3 + 0.46SiO_2$ $0.68Al_2O_3 + 0.32MgO \leftrightarrow SiO_2$	70 20	1550	Richter et al. (1998)
CMAS	$CaO \leftrightarrow 0.36MgO + 0.32Al_2O_3 + 0.32SiO_2$ $MgO \leftrightarrow 0.07CaO + 0.53Al_2O_3 + 0.4SiO_2$ $0.13CaO + 0.26MgO + 0.61Al_2O_3 \leftrightarrow SiO_2$	59 26 3.2	1500	Richter et al. (1998)
NCAS	$Na_2O + 0.02Al_2O_3 \leftrightarrow 0.92CaO + 0.09SiO_2$ $CaO + 0.02Na_2O \leftrightarrow 0.47Al_2O_3 + 0.52SiO_2$ $CaO + 0.17SiO_2 \leftrightarrow 0.99Al_2O_3 + 0.15Na_2O$	29.5 0.58 0.3	1200	this study

Table 3: Diffusion eigenvectors and eigenvalues from the literature.

nant eigenvector found in CAS (Liang et al., 1996a) and MAS (Richter et al., 1998) compositions. Also, the two dominant eigenvectors of the CMAS system in (Richter et al., 1998) correspond to the exchange of alkaline-earth species with silica and alumina. Since the environment of aluminum is expected to be different with or without sodium, with a fraction of aluminum tetrahedra being compensated preferentially by sodium ions (Cormier and Neuville, 2004; Lee and Sung, 2008), it is quite surprising that the dominant eigenvector of the CAS system transposes to our NCAS system. A striking result of our study is therefore that in our quaternary system, the two most important eigenvectors of the diffusion matrix correspond to the dominant eigenvectors of the ternary sub-systems. This robustness of eigenvectors to compositional changes and the addition of new species could be used to design experimental strategies to determine the diffusion matrix of complex systems.

The slowest eigenvector in Table 2 corresponds to the exchange of calcium and aluminum oxides, with only small couplings with silica and sodium oxide. There is no direct equivalent of this eigenvector in the studies summarized in Table 3. However, our composition is richer in silica than most compositions of Table 3, in particular CAS compositions. Moreover, our third eigenvector is determined with much less accuracy than the other two, due to the large difference between the first and last eigenvalues. In order to improve the accuracy of the third eigenvector, diffusion couples with a zero projection on the first eigenvector would be required.

5.3. Microscopic interpretation of exchange reactions

Eigenvectors can be interpreted as exchange reactions between ions (Chakraborty et al., 1995b), converting first from weight concentration to molar concentration of oxides, and from oxide to ionic concentration. This conversion results in the following reactions

$$\mathbf{v_1} : \mathrm{Na^+} + 0.01\mathrm{Al^{3+}} \leftrightarrow 0.5\mathrm{Ca^{2+}} + 0.04\mathrm{Si^{4+}} \qquad (15)$$

$$\mathbf{v_2} : \mathrm{Ca^{2+}} + 0.04\mathrm{Na^+} \leftrightarrow 0.52\mathrm{Al^{3+}} + 0.49\mathrm{Si^{4+}}. \qquad (16)$$

In the above equations, terms highlighted in blue have very small coefficients, and probably stem from numerical errors. Therefore, we neglect these terms in the following. Note that even if charge does not appear to be conserved in (16), charge is compensated by oxygen anions, not represented in the exchange reactions. Eq. (16) could equally be written as

$$\mathbf{v_2} : \mathrm{Ca^{2+}} + 0.04\mathrm{Na^+} \leftrightarrow 0.52\mathrm{Al^{3+}} + 0.49\mathrm{Si^{4+}} + 0.74\mathrm{O^{2-}}. \qquad (17)$$

However, it is interesting to observe that the fastest reaction (15) is charge-balanced by cations.

Equations such as (15) and (16) can be interpreted in terms of microscopic exchange reactions. For the first one involving one $\mathrm{Na^+}$ and half a $\mathrm{Ca^{2+}}$, a possible mechanism is illustrated on Fig. 7 (a), involving two silica tetrahedra. At the beginning of the exchange, one calcium ion is bound to two oxygens on two different tetrahedra, one of which has an additional non-bridging oxygen associated with a sodium ion (see Fig. 7 (a)). Let us suppose that the calcium ion breaks one of its two bonds to move closer to the sodium ion, and that the sodium ion moves close to the oxygen ion initially bound to the calcium ion. At the end of the exchange, the calcium ion is bound to two oxygen ions of the same tetrahedron, while the sodium ion is a modifier of a different tetrahedron than initially. This sequence is a possible mechanism to account for reaction (15). The exchange of sodium and calcium is likely to take place in the so-called Greaves channels (Greaves, 1985; Jund et al., 2001; Meyer et al., 2002; Bauchy and Micoulaut, 2011; Tilocca, 2010). Moreover, this mechanism involves only non-bridging oxygens, so that no $\mathrm{Si-O}$ or $\mathrm{Al-O}$ bound is broken. Therefore, such exchanges are more frequent than reactions involving network formers, as (16).

As for the second eigenvector, we have sketched a possible mechanism in Fig. 7 (b). The proposed exchange involves two silicon tetrahedron and one aluminum, that is 4-coordinated at the beginning and at the end of the reaction. The aluminum is charge-compensated by a calcium ion, that also acts as a modifier for one of the silicon tetrahedron. Then, the aluminum becomes 5-coordinated when a new $\mathrm{Al-O-Si}$ is formed, and the calcium only compensates the aluminum (Fig. 7 (b) center). Finally, the calcium moves closer to another silicon tetrahedron and break an $\mathrm{Al-O-Si}$ bond in order to act both as a modifier and charge compensator. This exchange describes how calcium progresses through the network of silicon and aluminum tetrahedra by breaking $\mathrm{Al-O-Si}$ bonds, and is therefore consistent with the exchange

$$\mathrm{Ca^{2+}} \leftrightarrow 0.5\mathrm{Al^{3+}} + 0.5\mathrm{Si^{4+}}. \qquad (18)$$

As for network formers, the above reaction requires to break a $\mathrm{Al-O}$ bound, which takes more time than breaking a chemical bound between oxygen and a network modifier. Therefore, the frequency of the second

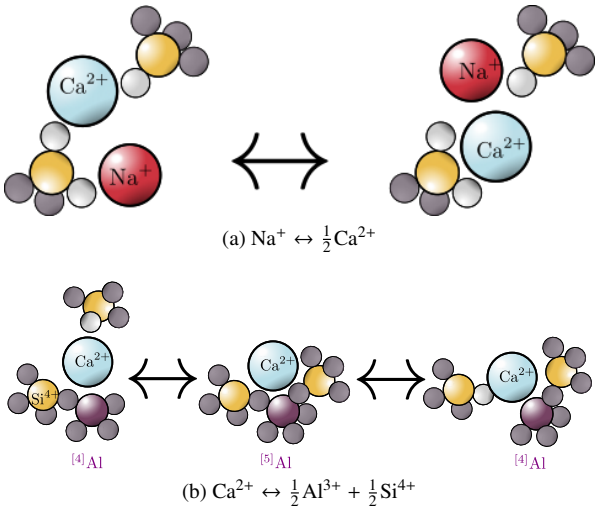

Figure 7: Schematic drawing of local exchanges with a stoechiometry corresponding to eigenvectors of the diffusion matrix. Sodium cations are represented in red, calcium in blue, silicon in yellow, aluminum in purple, bridging oxygens in dark gray and non-bridging oxygens in light grey. (a) Exchange between sodium and calcium, corresponding to Eq. (15). (b) Exchange between calcium, and silicon and aluminum, corresponding to Eq. (16).

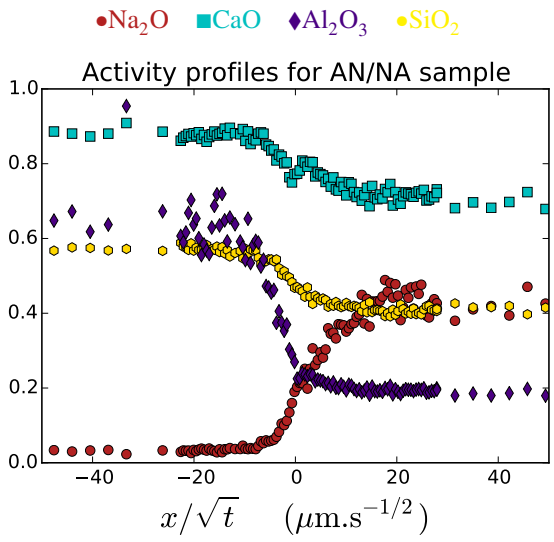

Figure 8: Activity profiles for the AN/NA sample, for a heat treatment of 1h at 1200°C. In order to represent all activity profiles on the same plot, we have used arbitrary scaling coefficients and represented $10^9 \times a(Na_2O)$, $2.10^4 \times a(CaO)$ and $5.10^4 \times a(Al_2O_3)$.

reaction mechanism is expected to be much lower than for the first exchange, in agreement with experimental eigenvalues.

We have not attempted to find a reaction mechanism for the third eigenvector, since we believe that the uncertainty on the direction of the eigenvector is large, because of the ill-conditioning of the diffusion matrix.

We do not claim that the reactions sketched in Fig. 7 are the only possible exchanges leading to the stoechiometry of Eqs. (15-16). It is possible that other configurations could result in a similar chemical balance. However, writing diffusion eigenvectors as simple local exchanges has several advantages. First, identifying such exchanges makes it possible to look for their signature using either molecular-dynamics or ab-initio simulations (Tilocca, 2010) or exchange rates computed from *in situ* NMR measurements (Stebbins et al., 1995; Gruener et al., 2001; Kanehashi and Stebbins, 2007). Second, identifying possible configurations responsible for the chemical exchanges helps to understand why the direction of eigenvectors does not vary much with composition (Liang et al., 1996a): if a discrete number of possible exchanges dominates mass transport, eigenvectors of the diffusion matrix should correspond to the most frequent exchanges and be invariant over concentration domains where the frequency ranking of reactions stays the same.

5.4. *Activity variations across diffusion profiles*

From a thermodynamic perspective, diffusion of a given species is driven by the gradient in the activity of that species, rather than its concentration (Liang et al., 1997). In other words, phenomena such as the uphill diffusion of Ca described here and in the literature (e.g. (Zhang et al., 1989; Liang et al., 1996a)) may be considered as the macroscopic consequence of significant variations in activity coefficient across a given diffusion profile. In this case, the complex variations in concentration should correspond to a simple variation in activity across the profile, with no local extrema in the latter. Direct determination of the relevant activity coefficients has not been made in the portion of the quaternary system studied here, but thermodynamic models available in the literature may be used to estimate how activities vary across our diffusion profiles. For this purpose we have used the FactSage programme (Bale et al., 2002, 2009), a commercially available thermodynamic calculator constructed from databases in systems of increasing compositional complexity. We note that in almost all cases smooth and continuous variations in activity (with no maxima) are calculated across our profiles for all elements. For example, for the diffusion couple AN/NA, which shows the most prominent uphill diffusion of calcium concentration (c.f. Fig. 4a), calculated activities of CaO (Fig. 8) indicate that: i) despite the fact that initial concentrations of CaO were identi-

cal across the profile, the activity of CaO was different in each starting glass, and ii) that a perfectly continuous decrease in CaO activity is calculated, a behaviour also found for the three other oxide components in this sample (Fig. 8). A detailed analysis and interpretation of all the calculated activities derived from our data-set is outside the scope of the present contribution, but this preliminary analysis clearly shows that consideration of oxide activities may be used to rationalize even highly non-linear concentration gradients that show multiple extrema.

5.5. Geological implications

Assuming that eigenvectors are not a significant function of temperature, the results obtained here provide some qualitative insights into the conditions that would favour uphill diffusion in geological systems (i.e. that will lead to concentration profiles that cannot be considered in terms of effective binary diffusion). For example, we find that complex gradients in Ca content are generated when sodium diffuses against network-forming cations such as Si and Al (Fig. 4). However, this situation is not commonly encountered in geological systems. For example, dissolution of very Ca-rich plagioclase may result in opposing concentration gradients of Na and Al around dissolving grains, but in that case there will also be significant gradients in Ca that may obscure the effects of off-diagonal terms of the diffusion matrix. Furthermore, for the case of the Moon (one of the most potentially important contexts for anorthite dissolution) the concentrations of Na are so low that no non-linear effects on Ca-diffusion have been described (e.g. (Morgan et al., 2006)). On the other hand, dissolution of albite-rich plagioclase should result in strong gradients of Na with only weak associated gradients of CaO. However, in this case, gradients of Na, Si and Al may all be positively correlated around the dissolving grain, again limiting the development of uphill diffusion of Ca. We do note, however, that weak up-hill gradients have been described around dissolving plagioclase grains (in SiO_2 for the experiments of (Morgan et al., 2006), and Na_2O for (Yu et al., 2016)) indicating that knowledge of the complete diffusion matrix is necessary when modeling the detailed behaviour of geological systems. However, we also stress that quantitative application of our results to systems of geochemical interest must await quantification of the temperature dependence of the diffusion matrix and confirmation that the eigenvectors derived here are indeed applicable over relevant temperature ranges.

Conclusion

Using diffusion-couple experiments, we determined the diffusion matrix in the soda-lime aluminosilicate system, in the vicinity of a composition of 64.5 wt%SiO_2 , 13.3 wt%Na_2O, 10.8 wt%CaO, 11.4 wt%Al_2O_3. We used a large number of diffusion experiments in order to overconstrain the determination of the diffusion matrix, for a better robustness to measurement noise and ill-conditioning of the matrix. Indeed, we found a factor of 50 between the largest eigenvalue, corresponding to the exchange of sodium and calcium, and the second largest eigenvalue, corresponding to an exchange involving network formers. Our study therefore showed that the diffusion of sodium is largely decoupled from that of network formers, since sodium only appears in the exchange reaction with calcium.

This first study of multicomponent diffusion in a quaternary aluminosilicate glass containing both alkali and alkaline-earth cations permits comparisons with previous studies in ternary systems. The dominant eigenvector, corresponding to the exchange of sodium and calcium, plays the same role in our quaternary system as in the ternary soda-lime system. Moreover, the second eigenvector, corresponding to the exchange of calcium with network formers, is the dominant eigenvector in ternary CAS systems. The diffusion matrix of the NAS system has not been determined yet in the literature, but the eigenvectors of the KAS system (transposing Na for K) do not seem to play a role in the NCAS system. Indeed, we observed in our system a calcium-mediated decoupling between sodium and network formers. Future studies adding a fifth element, such as magnesium or potassium, could reveal the extent to which complex systems can be modeled using a decomposition in simpler systems.

Finally, the ability to model diffusion over a large composition domain with a single set of eigenvectors and eigenvalues, and the persistence of eigenvectors with the addition of elements, suggests that eigenvectors can be interpreted as cooperative rearrangements of multiple species. We attempted to give a microscopic interpretation of these rearrangements. In order to probe the existence of such mechanisms at the atomic level, molecular dynamics would be required, in order to extract collective dynamic patterns responsible for the diffusion of species.

Acknowledgments

The authors gratefully acknowledge the experimental help of Séverine Bellayer, Sabrina Simoes and Erick

Lamotte, as well as enlightening discussions with Jean-Marc Flesselles and William Woelffel.

References

Acosta-Vigil, A., London, D., Dewers, T. A., Morgan, G. B., 2002. Dissolution of corundum and andalusite in H_2O-saturated haplogranitic melts at 800° C and 200 MPa: constraints on diffusivities and the generation of peraluminous melts. Journal of Petrology 43 (10), 1885–1908.

Acosta-Vigil, A., London, D., Morgan, G. B., Dewers, T. A., 2006. Dissolution of quartz, albite, and orthoclase in H_2O-saturated haplogranitic melt at 800° C and 200 MPa: Diffusive transport properties of granitic melts at crustal anatectic conditions. Journal of Petrology 47 (2), 231–254.

Bale, C., Bélisle, E., Chartrand, P., Decterov, S., Eriksson, G., Hack, K., Jung, I.-H., Kang, Y.-B., Melançon, J., Pelton, A., et al., 2009. Factsage thermochemical software and databases—recent developments. Calphad 33 (2), 295–311.

Bale, C., Chartrand, P., Degterov, S., Eriksson, G., Hack, K., Mahfoud, R. B., Melançon, J., Pelton, A., Petersen, S., 2002. Factsage thermochemical software and databases. Calphad 26 (2), 189–228.

Bauchy, M., Micoulaut, M., 2011. From pockets to channels: Density-controlled diffusion in sodium silicates. Physical Review B 83 (18), 184118.

Behrens, H., Stelling, J., 2011. Diffusion and redox reactions of sulfur in silicate melts. Reviews in Mineralogy and Geochemistry 73 (1), 79–111.

Bottinga, Y., Weill, D., Richet, P., 1982. Density calculations for silicate liquids. i. revised method for aluminosilicate compositions. Geochimica et Cosmochimica Acta 46 (6), 909–919.

Brady, J. B., 1995. Diffusion data for silicate minerals, glasses, and liquids. Mineral physics & crystallography: A handbook of physical constants, 269–290.

Chakraborty, S., Dingwell, D. B., Rubie, D. C., 1995a. Multicomponent diffusion in ternary silicate melts in the system K_2O–Al_2O_3–SiO_2: I. experimental measurements. Geochimica et Cosmochimica Acta 59 (2), 255–264.

Chakraborty, S., Dingwell, D. B., Rubie, D. C., 1995b. Multicomponent diffusion in ternary silicate melts in the system K_2O–Al_2O_3–SiO_2: II. mechanisms, systematics, and geological applications. Geochimica et Cosmochimica Acta 59 (2), 265–277.

Chen, Y., Zhang, Y., 2008. Olivine dissolution in basaltic melt. Geochimica et Cosmochimica Acta 72 (19), 4756–4777.

Chopinet, M.-H., Rouyer, E., Gaume, O., Dec. 25 2001. Glass composition and chemically tempered glass substrate. US Patent 6,333,285.

Cooper, R. F., Fanselow, J. B., Poker, D. B., 1996. The mechanism of oxidation of a basaltic glass: chemical diffusion of network-modifying cations. Geochimica et Cosmochimica Acta 60 (17), 3253–3265.

Cormier, L., Neuville, D., 2004. Ca and Na environments in Na2O–CaO–Al2O3–SiO2 glasses: influence of cation mixing and cation-network interactions. Chemical geology 213 (1), 103–113.

Danielson, P. S., DeMartino, S. E., Drake, M. A., Morena, R. M., Pal, S., Schaut, R. A., May 17 2016. Glass compositions with improved chemical and mechanical durability. US Patent 9,340,447.

de Koker, N., Stixrude, L., 2010. Theoretical computation of diffusion in minerals and melts. Reviews in Mineralogy and Geochemistry 72 (1), 971–996.

Eagan, R. J., Swearekgen, J., 1978. Effect of composition on the mechanical properties of aluminosilicate and borosilicate glasses. Journal of the American Ceramic Society 61 (1-2), 27–30.

Edwards, B., Russell, J., 1996. A review and analysis of silicate mineral dissolution experiments in natural silicate melts. Chemical Geology 130 (3), 233–245.

Fluegel, A., Earl, D. A., Varshneya, A. K., Seward, T. P., 2008. Density and thermal expansion calculation of silicate glass melts from 1000 c to 1400 c. Physics and Chemistry of Glasses-European Journal of Glass Science and Technology Part B 49 (5), 245–257.

Greaves, G., 1985. Exafs and the structure of glass. Journal of Non-Crystalline Solids 71 (1), 203–217.

Gruener, G., Odier, P., Meneses, D. D. S., Florian, P., Richet, P., 2001. Bulk and local dynamics in glass-forming liquids: a viscosity, electrical conductivity, and nmr study of aluminosilicate melts. Physical Review B 64 (2), 024206.

Gupta, P., Cooper, A., 1971. The [D] matrix for multicomponent diffusion. Physica 54 (1), 39–59.

Imre, Á. W., Voss, S., Mehrer, H., 2002. Ionic transport in $0.2[x\mathrm{Na_2O}(1-x)\mathrm{Rb_2O}]0.8\mathrm{B_2O_3}$ mixed-alkali glasses. Physical Chemistry Chemical Physics 4 (14), 3219–3224.

Isard, J., 1969. The mixed alkali effect in glass. Journal of Non-Crystalline Solids 1 (3), 235–261.

Jambon, A., 1982. Tracer diffusion in granitic melts: experimental results for Na, K, Rb, Cs, Ca, Sr, Ba, Ce, Eu to 1300° C and a model of calculation. Journal of Geophysical Research: Solid Earth (1978–2012) 87 (B13), 10797–10810.

Jambon, A., Carron, J.-P., 1976. Diffusion of Na, K, Rb and Cs in glasses of albite and orthoclase composition. Geochimica et Cosmochimica Acta 40 (8), 897–903.

Jund, P., Kob, W., Jullien, R., 2001. Channel diffusion of sodium in a silicate glass. Physical Review B 64 (13), 134303.

Kanehashi, K., Stebbins, J. F., 2007. In situ high temperature 27 Al NMR study of structure and dynamics in a calcium aluminosilicate glass and melt. Journal of Non-Crystalline Solids 353 (44), 4001–4010.

Karlsson, S., Jonson, B., Stålhandske, C., 2010. The technology of chemical glass strengthening–a review. Glass Technology-European Journal of Glass Science and Technology Part A 51 (2), 41–54.

Kjeldsen, J., Smedskjaer, M. M., Mauro, J. C., Youngman, R. E., Huang, L., Yue, Y., 2013. Mixed alkaline earth effect in sodium aluminosilicate glasses. Journal of Non-Crystalline Solids 369, 61–68.

Kress, V., Ghiorso, M., 1993. Multicomponent diffusion in MgO–Al_2O_3–SiO_2 and CaO–MgO–Al_2O_3–SiO_2 melts. Geochimica et Cosmochimica Acta 57 (18), 4453–4466.

Kress, V. C., Ghiorso, M. S., 1995. Multicomponent diffusion in basaltic melts. Geochimica et Cosmochimica Acta 59 (2), 313–324.

LaTourrette, T., Wasserburg, G., Fahey, A., 1996. Self diffusion of Mg, Ca, Ba, Nd, Yb, Ti, Zr, and U in haplobasaltic melt. Geochimica et Cosmochimica Acta 60 (8), 1329–1340.

Lee, S. K., Sung, S., 2008. The effect of network-modifying cations on the structure and disorder in peralkaline Ca–Na aluminosilicate glasses: O-17 3QMAS NMR study. Chemical Geology 256 (3), 326–333.

Lesher, C., 1994. Kinetics of Sr and Nd exchange in silicate liquids: theory, experiments, and applications to uphill diffusion, isotopic equilibration, and irreversible mixing of magmas. Journal of Geophysical Research: Solid Earth (1978–2012) 99 (B5), 9585–9604.

Lesher, C. E., 2010. Self-diffusion in silicate melts: theory, observations and applications to magmatic systems. Reviews in Mineralogy and Geochemistry 72 (1), 269–309.

Liang, Y., 1999. Diffusive dissolution in ternary systems: analysis with applications to quartz and quartzite dissolution in molten silicates. Geochimica et Cosmochimica Acta 63 (23), 3983–3995.

Liang, Y., 2010. Multicomponent diffusion in molten silicates: theory,

experiments, and geological applications. Reviews in Mineralogy and Geochemistry 72 (1), 409–446.

Liang, Y., Davis, A. M., 2002. Energetics of multicomponent diffusion in molten $CaO-Al_2O_3-SiO_2$. Geochimica et cosmochimica acta 66 (4), 635–646.

Liang, Y., Richter, F. M., Chamberlin, L., 1997. Diffusion in silicate melts: Iii. empirical models for multicomponent diffusion. Geochimica et Cosmochimica Acta 61 (24), 5295–5312.

Liang, Y., Richter, F. M., Davis, A. M., Watson, E. B., 1996a. Diffusion in silicate melts: I. self diffusion in $CaO - Al_2O_3 - SiO_2$ at 1500° C and 1 GPa. Geochimica et Cosmochimica Acta 60 (22), 4353–4367.

Liang, Y., Richter, F. M., Watson, E. B., 1994. Convection in multicomponent silicate melts driven by coupled diffusion. Nature 369 (6479), 390–392.

Liang, Y., Richter, F. M., Watson, E. B., 1996b. Diffusion in silicate melts: Ii. multicomponent diffusion in $CaO-Al_2O_3-SiO_2$ at 1500° C and 1 GPa. Geochimica et Cosmochimica Acta 60 (24), 5021–5035.

Lundstrom, C., 2003. An experimental investigation of the diffusive infiltration of alkalis into partially molten peridotite: implications for mantle melting processes. Geochemistry, Geophysics, Geosystems 4 (9), 1.

Mazurin, O. V., Porai-Koshits, E., 1984. Phase separation in glass. Elsevier.

Meyer, A., Schober, H., Dingwell, D., 2002. Structure, structural relaxation and ion diffusion in sodium disilicate melts. EPL (Europhysics Letters) 59 (5), 708.

Morgan, Z., Liang, Y., Hess, P., 2006. An experimental study of anorthosite dissolution in lunar picritic magmas: implications for crustal assimilation processes. Geochimica et Cosmochimica Acta 70 (13), 3477–3491.

Mungall, J. E., 2002. Empirical models relating viscosity and tracer diffusion in magmatic silicate melts. Geochimica et Cosmochimica Acta 66 (1), 125–143.

Mungall, J. E., Romano, C., Dingwell, D. B., 1998. Multicomponent diffusion in the molten system $K_2O-Na_2O-Al_2O_3-SiO_2-H_2O$. American Mineralogist 83 (7), 685–699.

Ni, H., Hui, H., Steinle-Neumann, G., 2015. Transport properties of silicate melts. Reviews of Geophysics.

Njiokep, E. T., Imre, A., Mehrer, H., 2008. Tracer diffusion of 22 Na and 45 Ca, ionic conduction and viscosity of two standard soda-lime glasses and their undercooled melts. Journal of Non-Crystalline Solids 354 (2), 355–359.

Oishi, Y., Cooper, A., Kingery, W., 1965. Dissolution in ceramic systems: III, boundary layer concentration gradients. Journal of the American Ceramic Society 48 (2), 88–95.

Oishi, Y., Nanba, M., Pask, J. A., 1982. Analysis of liquid-state interdiffusion in the system $CaO-Al_2O_3-SiO_2$ using multiatomic ion models. Journal of the American Ceramic Society 65 (5), 247–253.

Priven, A., 2004. General method for calculating the properties of oxide glasses and glass forming melts from their composition and temperature. Glass Technology-European Journal of Glass Science and Technology Part A 45 (6), 244–254.

Richter, F. M., Liang, Y., Davis, A. M., 1999. Isotope fractionation by diffusion in molten oxides. Geochimica et Cosmochimica Acta 63 (18), 2853–2861.

Richter, F. M., Liang, Y., Minarik, W. G., 1998. Multicomponent diffusion and convection in molten $MgO-Al_2O_3-SiO_2$. Geochimica et Cosmochimica Acta 62 (11), 1985–1991.

Richter, F. M., Watson, E. B., Mendybaev, R. A., Teng, F.-Z., Janney, P. E., 2008. Magnesium isotope fractionation in silicate melts by chemical and thermal diffusion. Geochimica et Cosmochimica Acta 72 (1), 206–220.

Roling, B., Ingram, M., 2000. Mixed alkaline–earth effects in ion conducting glasses. Journal of non-crystalline solids 265 (1), 113–119.

Roskosz, M., Toplis, M. J., Richet, P., 2005. Experimental determination of crystal growth rates in highly supercooled aluminosilicate liquids: Implications for rate-controlling processes. American Mineralogist 90 (7), 1146–1156.

Roskosz, M., Toplis, M. J., Richet, P., 2006. Kinetic vs. thermodynamic control of crystal nucleation and growth in molten silicates. Journal of non-crystalline solids 352 (2), 180–184.

Saggioro, B., Ziemath, E., 2006. Diffusion coefficient of K+ in ion exchanged glasses calculated from the refractive index and the vickers hardness profiles. Journal of non-crystalline solids 352 (32), 3567–3571.

Samaddar, B., Kingery, W., Cooper, A., 1964. Dissolution in ceramic systems: II, dissolution of alumina, mullite, anorthite, and silica in a calcium-aluminum-silicate slag. Journal of the American Ceramic Society 47 (5), 249–254.

Sandhage, K. H., Yurek, G. J., 1990. Direct and indirect dissolution of sapphire in calcia–magnesia–alumina–silica melts: dissolution kinetics. Journal of the American Ceramic Society 73 (12), 3633–3642.

Schaeffer, H. A., 1984. Diffusion-controlled processes in glass forming melts. Journal of non-crystalline solids 67 (1), 19–33.

Smith, D. R., Cooper, R. F., 2000. Dynamic oxidation of a Fe 2+-bearing calcium–magnesium–aluminosilicate glass: the effect of molecular structure on chemical diffusion and reaction morphology. Journal of non-crystalline solids 278 (1), 145–163.

Spera, F. J., 2000. Physical properties of magma. Encyclopedia of volcanoes, 171–190.

Spera, F. J., Yuen, D. A., Kemp, D. V., 1984. Mass transfer rates along vertical walls in magma chambers and marginal upwelling. Nature 310, 764–767.

Stebbins, J., Sen, S., Farnan, I., 1995. Silicate species exchange, viscosity, and crystallization in a low-silica melt: In situ high-temperature MAS NMR spectroscopy. American Mineralogist 80 (7), 861–864.

Sugawara, H., Nagata, K., Goto, K., 1977. Interdiffusivities matrix of $CaO-Al_2O_3-SiO_2$ melt at 1723 k to 1823 k. Metallurgical Transactions B 8 (3), 605–612.

Swenson, J., Adams, S., 2003. Mixed alkali effect in glasses. Physical review letters 90 (15), 155507.

Tilocca, A., 2010. Sodium migration pathways in multicomponent silicate glasses: Car–Parrinello molecular dynamics simulations. The Journal of chemical physics 133 (1), 014701.

Trial, A. F., Spera, F. J., 1994. Measuring the multicomponent diffusion matrix: Experimental design and data analysis for silicate melts. Geochimica et Cosmochimica Acta 58 (18), 3769–3783.

Varshneya, A., Cooper, A., 1972. Diffusion in the system $K_2O-SrO-SiO_2$: III, interdiffusion coefficients*. Journal of the American Ceramic Society 55 (6), 312–317.

Vielzeuf, D., Saúl, A., 2011. Uphill diffusion, zero-flux planes and transient chemical solitary waves in garnet. Contributions to Mineralogy and Petrology 161 (5), 683–702.

Wakabayashi, H., Oishi, Y., 1978. Liquid-state diffusion of $Na_2O-CaO-SiO_2$ system. The Journal of Chemical Physics 68 (5), 2046–2052.

Wu, X., Moskowitz, J. D., Mauro, J. C., Potuzak, M., Zheng, Q., Dieckmann, R., 2012. Sodium tracer diffusion in sodium boroaluminosilicate glasses. Journal of Non-Crystalline Solids 358 (12), 1430–1437.

Yu, Y., Zhang, Y., Yang, C., 2016. Kinetics of anorthite dissolution in basaltic melt. Geochimica et Cosmochimica Acta 1 (1), 1.

Zhang, Y., 2010. Diffusion in minerals and melts: theoretical background. Reviews in Mineralogy and Geochemistry 72 (1), 5–59.

Zhang, Y., Ni, H., Chen, Y., 2010. Diffusion data in silicate melts. Reviews in Mineralogy and Geochemistry 72 (1), 311–408.

978 Zhang, Y., Walker, D., Lesher, C. E., 1989. Diffusive crystal dissolu-
979 tion. Contributions to Mineralogy and Petrology 102 (4), 492–513.